Biodegradation (2014) 25:351–371
DOI 10.1007/s10532-013-9665-y

ORIGINAL ARTICLE

Model based evaluation of a contaminant plume development under aerobic and anaerobic conditions in 2D bench-scale tank experiments

E. Ballarini · C. Beyer · R. D. Bauer · C. Griebler · S. Bauer

Received: 17 April 2013 / Accepted: 4 October 2013 / Published online: 13 October 2013

Abstract The influence of transverse mixing on competitive aerobic and anaerobic biodegradation of a hydrocarbon plume was investigated using a two-dimensional, bench-scale flow-through laboratory tank experiment. In the first part of the experiment aerobic degradation of increasing toluene concentrations was carried out by the aerobic strain *Pseudomonas putida* F1. Successively, ethylbenzene (injected as a mixture of unlabeled and fully deuterium-labeled isotopologues) substituted toluene; nitrate was added as additional electron acceptor and the anaerobic denitrifying strain *Aromatoleum aromaticum* EbN1 was inoculated to study competitive degradation under aerobic / anaerobic conditions. The spatial distribution of anaerobic degradation was resolved by measurements of compound-specific stable isotope fractionation induced by the anaerobic strain as well as compound concentrations. A fully transient numerical reactive transport model was employed and calibrated using measurements of electron donors, acceptors and isotope fractionation. The aerobic phases of the experiment were successfully reproduced using a double Monod kinetic growth model and assuming an initial homogeneous distribution of *P. putida* F1. Investigation of the competitive degradation phase shows that the observed isotopic pattern cannot be explained by transverse mixing driven biodegradation only, but also depends on the inoculation process of the anaerobic strain. Transient concentrations of electron acceptors and donors are well reproduced by the model, showing its ability to simulate transient competitive biodegradation.

Keywords Competitive biodegradation · Isotope fractionation · Numerical modeling · Transverse mixing

E. Ballarini (✉) · C. Beyer · S. Bauer
Institute of Geosciences, University of Kiel, Ludewig-Meyn-Str. 10, 24118 Kiel, Germany
e-mail: ballarin@gpi.uni-kiel.de

R. D. Bauer · C. Griebler
Institute of Groundwater Ecology, Helmholtz Zentrum München, Ingolstaedter Landstr. 1, 85764 Neuherberg, Germany

Introduction

Release of organic pollutants into the environment and especially in groundwater often causes persistent contamination and adversely affects drinking water resources. A thorough understanding of the physical, chemical and microbiological processes determining the pollutant fate is a requirement for quantifying the environmental impact as well as remediation options.

Natural attenuation plays an important role for removal of these contaminants and monitored natural attenuation has been implemented in various national water legislations as a possible remediation alternative

(Declercq et al. 2012). Natural attenuation can be an option if sufficient removal of contaminants is demonstrated. Among the processes governing the fate and transport of these pollutants, only biodegradation decreases the total contaminant mass. Several approaches are commonly used for estimating biodegradation rates in groundwater at contaminated sites, including mass balance calculations (e.g. Bockelmann et al. 2003; Peter et al. 2004), in situ microcosm studies (e.g. Gillham et al. 1990; Stelzer et al. 2006), and the analysis of concentration-distance relations along the plume center line (Chapelle et al. 1996; Wiedemeier et al. 1999; Bauer et al. 2006; Beyer et al. 2007). An alternative strategy for monitoring in situ biodegradation is to analyze the spatio-temporal changes in stable isotope composition of the compound of interest (Sherwood Lollar et al. 1999; Meckenstock et al. 2004; Schmidt et al. 2004; Hunkeler et al. 2005; Blum et al. 2009).

However, a thorough process understanding is difficult to obtain from field data alone, because field studies often lack the detailed data at the required small scale to spatially and temporally resolve the ongoing processes and effects. Thus, laboratory scale experiments are required for studying and quantifying the individual transport and reaction processes. For example, bench scale tank experiments have shown the effects of transverse dispersion on mixing, and proven the small value of the transverse dispersivity (Klenk and Grathwohl 2002; Olsson and Grathwohl 2007; Ballarini et al. 2012). Isotope fractionation due to biodegradation, together with the degradation pathways of individual substances, the microbial consortia involved and terminal-electron-accepting processes, have all been investigated in numerous controlled laboratory studies and shown the vast multitude of specific effects due to individual reaction pathways and microbial communities (e.g. Hunkeler et al. 2001; Mancini et al. 2003; Meckenstock et al. 1999; Morasch et al. 2001, 2002). However, these experiments typically are performed for well mixed batch systems. Therefore, the combined effects of physical transport and biodegradation has to be studied in transient flow-through experiments, which are well controlled and resemble more closely the ongoing processes at contaminated sites. Microbial degradation of organic contaminants hence was investigated in a number two-dimensional lab scale flow-through systems of different sizes, porous materials and configurations (e.g. Thullner et al. 2002; Huang et al. 2003; Nambi et al. 2003).

Advances in measurement techniques and experimental evaluation procedures (e.g. non-invasive quantifications solute concentrations) allow for increasingly complex experiments and an extraction of more detailed observation data. Bauer et al. (2009a) performed a 74 days long laboratory 2D bench-scale flow-through tank experiment, where biodegradation of BTEX was investigated under varying redox conditions. This kind of experiment thus allows studying the combined effects of transport and biodegradation reactions using a highly controlled laboratory model system of an organic contaminant in porous media. The main aim of Bauer et al. (2009a) study was to experimentally investigate the plume fringe concept (Wiedemeier et al. 1999; Thornton et al. 2001; Tuxen et al. 2006; Watson et al. 2005) which assumes that pollutants biodegradation in porous media is mainly mixing-controlled. The experiment consists of a number of transient phases, in which first aerobic degradation of toluene by *Pseudomunas putida* F1 under varying toluene concentrations is investigated. In later phases, competitive aerobic–anaerobic biodegradation of isotopically labelled ethylbenzene with nitrate as an additional electron acceptor and the denitrifying strain *Aromatoleum aromaticum* EbN1 is investigated, again under temporally varying concentrations of ethylbenzene and nitrate.

Interpretation of the results was mainly qualitative, accompanied by reactive transport simulations using a simplified hybrid analytical–numerical modelling approach, which assumed steady state conditions, considered only two of the 11 experimental phases, could only account for a single degradation pathway and could not evaluate the isotopic data. Rolle et al. (2010) used a comparable but shorter and less complex experiment (i.e. without transient phases of increasing electron donor concentrations and without switching the electron donor) and fitted isotopic patterns using a numerical transport and biodegradation model, now accounting for isotope fractionation and compound specific transverse dispersion. A full investigation of the coupled effects of transport and biodegradation under transient conditions with different electron donors and competitive biodegradation has therefore not been undertaken.

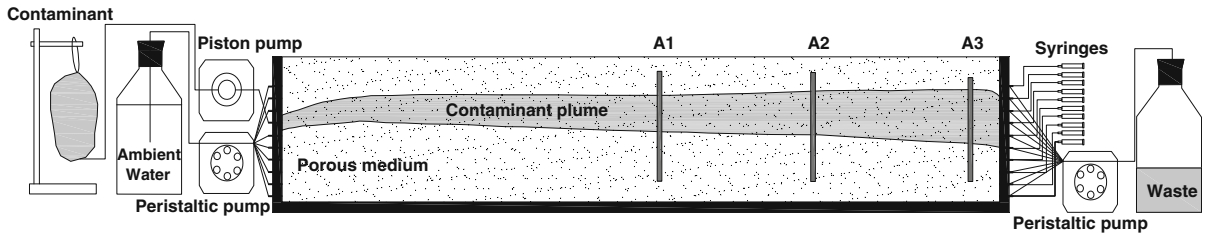

Fig. 1 Experimental set-up showing the contaminant plume after the injection of the carbon source from port 7. Flow is from left to right and it is maintained through peristaltic pumps, which inject oxidizing water from the inlet ports. Samples at the outlet are collected using ten syringes while oxygen concentration is measured at strips *A1*, *A2* and *A3* (modified from Bauer et al. 2009b)

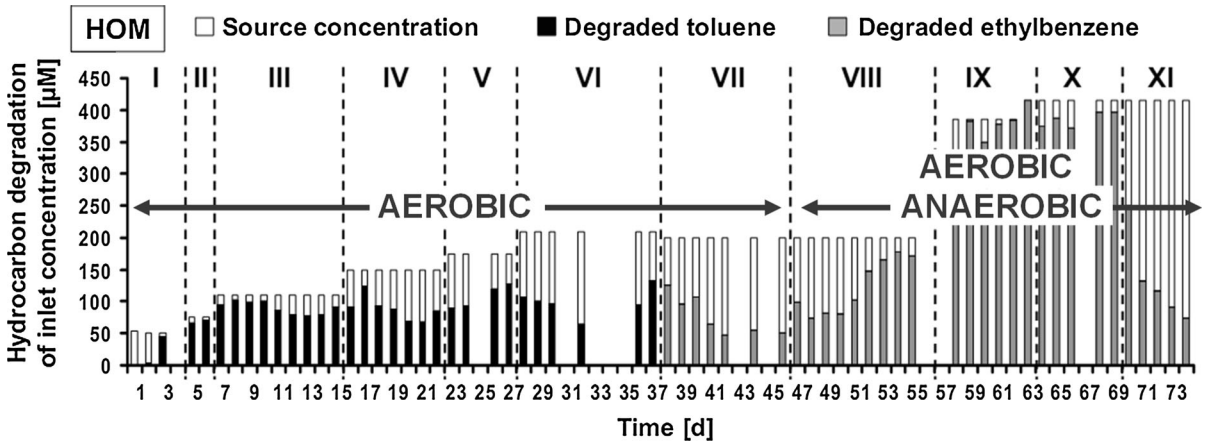

Fig. 2 Summary of the eleven phases of the experiment. *White bars* show the hydrocarbon concentration at port 7, in *black* the total toluene degraded and in *gray* the ethylbenzene at the outlet ports. At the beginning of Phase VII toluene was substituted by ethylbenzene, while in Phase VIII the denitrifying strain *A. aromaticum* EbN1 was inoculated (modified from Bauer et al. 2009a)

In this study, therefore, the effects of a transient supply of electron donors and acceptors and of single versus competitive biodegradation under transient conditions are investigated. The full dataset from the bench scale tank experiment of Bauer et al. (2009a), including transient phases as well as isotopic data, is available and used for this investigation. Numerical high resolution reactive transport modeling, and a consistent conceptual modeling approach are applied in our study to interpret the dataset of Bauer et al. (2009a). The developed model includes now all aerobic toluene and ethylbenzene degradation phases that precede the concurrent aerobic–anaerobic biodegradation phase, both pathways of concurrent aerobic and anaerobic ethylbenzene degradation, as well as the isotope fractionation process.

Materials and methods

Experimental set-up

The experiment investigated in this work is described in detail in Bauer et al. (2009a), therefore here only the main characteristics of the experimental set-up are summarized. The experiment was performed in a quasi 2D microcosm, which consists of a tank with inner dimensions of 77.3 × 1.04 × 14 cm^3 (Fig. 1) filled with sterile quartz sand (heated at 450 °C for 4 h) with a grain diameter of 0.2–0.3 mm (Aldrich, MO, USA). The 74 days long reactive transport experiment was divided in eleven phases, each characterized by different injected concentrations of the electron donor and acceptor (Fig. 2).

The flow field was established through 10 active ports placed at the inlet, while at the outlet side of the tank, 11 ports were active, of which the uppermost port was situated directly at the water table position and only collected negligible amounts of water. The flow rate was established by two peristaltic pumps (MCP, Ismatec, Glattbrugg, CH) attached to the ports at both sides of the tank and the transport velocity was determined by a bromide tracer test, resulting in 1.46 m day^{-1}.

Bromide was continuously injected in order to monitor and (if necessary) adjust the pumping in order to keep the flow field constant. All inlet ports were fed with an artificial groundwater medium. Nine of the ports were fed with an oxic medium containing nutrients and electron acceptors (oxygen and nitrate) but no carbon source, while one of the ports (port 7, from the bottom of the tank) was fed with a solution containing bromide as conservative tracer, nutrients and toluene. The latter was successively substituted by ethylbenzene as carbon source. For the exact composition of the artificial groundwater, see Bauer et al. (2009a). Concentrations of toluene, ethylbenzene, nitrate and bromide were measured in samples collected at the outlet ports by a multi-channel syringe pump (WPI, Berlin, Germany). Concentrations of bromide and nitrate were determined by ion chromatography (Dionex AS3500, Idstein, Germany), while toluene and ethylbenzene were measured by gas chromatography (Hewlett Packard 5890 series II; CA, USA). Additionally, oxygen concentrations were non-invasively recorded using oxygen-sensitive membrane strips attached to the inner tank wall at distances of 40, 57 and 74 cm from the inlet. Measurements of oxygen concentration were done by an optode technique (Microx 1 / FIBOX, PreSens, Regensburg, Germany).

Description of the experiment

Aerobic biodegradation (Phases I–VII)

Phases I–VI of the experiment comprised the aerobic degradation of toluene by the strain *P. putida* F1 according to the stoichiometry of metabolism given in Eq. (1), which (just as the reaction stoichiometries in Eqs. (2)–(4)) was derived using an approach of Kleerebezem and van Loosdrecht (2010)

$$C_7H_8 + 7.95O_2 + 2.6H_2O + 0.2NH_4^+ \rightarrow CH_{1.8}O_{0.5}N_{0.2} + 6.2H^+ + 6HCO_3^- \quad (1)$$

and where $CH_{1.8}O_{0.5}N_{0.2}$ is the assumed average stoichiometric composition of the biomass. The experiment started with the inoculation of the tank system with *P. putida* F1 (pulse injection of 6 h in port 6 and 8) and the simultaneous injection of toluene through port 7. The toluene concentration was kept constant within the individual phases of the experiment but progressively increased from initially 50 μmol l^{-1} in Phase I, to a final concentration of 210 μmol l^{-1} in Phase VI (Fig. 2). Additionally, all 10 inlet ports were constantly fed with a groundwater medium containing oxygen and nitrate at concentrations of 270 and 112 μmol l^{-1}, respectively.

At the beginning of Phase VII (day 37) toluene was substituted by a 3:1 mixture of unlabelled and labelled (fully deuterated) ethylbenzene (at concentration of 200 μmol l^{-1}) as electron donor and aerobically degraded by the *P. putida* F1 population established during the first six experimental phases (Eq. 2).

$$C_8H_{10} + 9.45O_2 + 2.6H_2O + 0.2NH_4^+ \rightarrow CH_{1.8}O_{0.5}N_{0.2} + 7.2H^+ + 7HCO_3^- \quad (2)$$

During Phase VII, no isotope fractionation from *P. Putida* F1 was observed from the ethylbenzene samples collected at the outlet ports (Bauer et al. 2009a).

Competitive biodegradation

At the beginning of Phase VIII (day 46) the denitrifying strain *A aromaticum* EbN1 (Rabus and Widdel 1995) was inoculated through ports 6 and 8 and the nitrate concentration in the groundwater medium was raised to a value of 1,350 μmol l^{-1}, while in port 7 concentration was kept one order of magnitude lower (112 μmol l^{-1}). Ethylbenzene was maintained at the same concentration as in Phase VII (200 μmol l^{-1}) and the competitive degradation (aerobic and anaerobic) of the contaminant was investigated.

The denitrifying strain used nitrate as electron acceptor to carry out the anaerobic oxidation of ethylbenzene, but as denitrification is a multi-step reaction process, different stoichiometries can be plausible depending if the reaction leads to the formation of intermediate products (NO_2^-, NO, N_2O) or in case of complete denitrification with the

conversion of nitrate to nitrogen. The two extreme reactions are therefore represented by Eq. (3), in the case of nitrate being converted to nitrogen and by Eq. (4), where nitrate is converted to nitrite.

$$C_8H_{10} + 7.56NO_3^- + 0.2NH_4^+ + 0.36H^+ \rightarrow CH_{1.8}O_{0.5}N_{0.2} + 3.78N_2 + 1.18H_2O + 7HCO_3^- \quad (3)$$

$$C_8H_{10} + 18.9NO_3^- + 0.2NH_4^+ + 2.6H_2O \rightarrow CH_{1.8}O_{0.5}N_{0.2} + 7.2H^+ + 18.9NO_2^- + 7HCO_3^- \quad (4)$$

The measured ratio of deuterium-labelled and unlabelled ethylbenzene isotopologues at the outlet ports was used to interpret the spatial distribution of the anaerobic degradation activity of *A. aromaticum* EbN1 (Bauer et al. 2009a).

Whereas *P. putida* F1 does not discriminate between the isotopologues, *A. aromaticum* EbN1 metabolizes the unlabelled substrate quicker than the deuterium-labelled ethylbenzene (ethylbenzene-*d10*), resulting in a fractionation, i.e. the accumulation of the latter in the undegraded residual. Before the inoculation of *A. aromaticum* EbN1 on day 46, no fractionation could be observed in the microcosms.

Numerical Model

The OpenGeoSys code (OGS; Kolditz et al. 2012a, b) was used for the simulation of this experiment. OGS has been applied for a number of groundwater flow and contaminant transport problems (e.g. Beyer et al. 2009; Rein et al. 2009) and is designed using object and process oriented software concepts (Kolditz and Bauer 2004). OGS solves the groundwater flow (Eq. 5) and transport equations (Eq. (6)) by standard Galerkin finite element methods by using semi-implicit finite differences (Crank–Nicholson scheme) for the time derivatives.

$$S\frac{\partial h}{\partial t} = \nabla(\mathbf{K}\nabla h) + q \quad (5)$$

$$\frac{\partial C}{\partial t} = -\mathbf{v_a}\nabla C + \nabla(\mathbf{D}\nabla C) + q_C \quad (6)$$

Here, S (m^{-1}) is the storage coefficient, h (m) is the piezometric head, $\mathbf{K}$ (m s^{-1}) is the tensor of hydraulic conductivity, q (s^{-1}) are source and sinks of water, C (mol m^{-3}) is the solute concentration, $\mathbf{D}$ (m^2 s^{-1}) is the hydrodynamic dispersion tensor and t (s) is the time. In Eq. (6) $\mathbf{v_a}$ (m s^{-1}) represents the vector of advective velocity, which is related to the Darcy velocity $\mathbf{u}$ (m s^{-1}) via the porosity n (–), i.e. $\mathbf{v_a} = \mathbf{u}/n = -\mathbf{K}\nabla h/n$, and thus represents the coupling term of Eq. (6) to Eq. (5). q_C (mol m^{-3} s^{-1}) is a solute source term including microbially mediated biogeochemical reactions. OGS uses a sequential non-iterative operator-splitting approach to couple the processes of groundwater flow, conservative transport and reactions. In contrast to Centler et al. (2010) or Li et al. (2013), where OGS was coupled to external reaction packages like BRNS or ChemApp, in this study biogeochemical reactions are quantified solely by OGS using a routine for solving stiff systems of ordinary differential equations (ODE). Generalized kinetic rate laws have been implemented in OGS to simulate rate limited processes such as microbial metabolism, inter-phase mass transfer [e.g. (non-linear) sorption or dissolution of non-aqueous-phase-liquids], and mineral dissolution/precipitation. Dynamics of microbial degraders is modeled by multiple Monod equations (e.g. Barry et al. 2002; Schäfer et al. 1998), as a combination of a growth and a linear decay term, and directly linked through a yield coefficient to substrate consumption.

The numerical model set-up applied to simulate the different phases of the experiment is, in principle, similar to the one used for the evaluation of a series of conservative tracer experiments in a comparable set-up described in Ballarini et al. (2012, 2013). The model domain used for the numerical investigation is a two-dimensional x–z oriented unconfined aquifer. Flow is from left to right, with a mean hydraulic gradient of 0.4 ‰, which is induced by Neumann conditions of specified flow to reproduce the pumping rate at the individual ports on the left and the right hand side of the model domain, while the bottom and top of the tank were treated as no flow boundaries. The contaminant source is represented by a fixed concentration boundary condition at the source position (port 7). The model domain consists of a two-dimensional finite element mesh of 90,061 nodes. The mesh was refined around the injection ports and along the plume region in order to minimize numerical dispersion, which is critical in regions of strongly diverging–converging flow and in the numerical simulation of mixing limited reactions.

For the biogeochemical system studied, growth of the microbial population X_P (mol_C m^{-3}) representing *P. putida* F1 (quantified as moles of organic carbon *C* bound in the biomass) by aerobic degradation of

toluene during experimental Phases I–VI can be described as

$$\frac{dX_P}{dt} = \mu_{\max}^{P,C_7H_8} X_P \frac{O_2}{M_{O_2}^{P,C_7H_8} + O_2} \frac{C_7H_8}{M_{C_7H_8}^{P} + C_7H_8} \frac{I_{X_P}}{I_{X_P} + X_P} - \xi_P X_P \quad (7)$$

where $\mu_{\max}^{P,C_7H_8}$ (s^{-1}) is the maximum growth rate of *P. putida* F1 on toluene, O_2 and C_7H_8 are the oxygen and toluene concentrations (mol m^{-3}), respectively, $M_{O_2}^{P,C_7H_8}$ and $M_{C_7H_8}^{P}$ are the corresponding Monod concentrations (mol m^{-3}) for toluene degradation by *P. putida* F1, and I_{X_P} (mol_C m^{-3}) is the maximum capacity (or biomass inhibition concentration). In lack of better knowledge on the exact mechanisms of bacterial inactivation, e.g. due to substrate shortage and bacterial decay, a simple first order rate with decay rate coefficient ξ_n (s^{-1}) was included in the model as a sink term for the bacteria. A similar equation can be derived for aerobic degradation of ethylbenzene by *P. putida* F1 (see the Appendix), Eq. (14), which does not discriminate between deuterated and non-deuterated ethylbenzene isotopologues, during experimental Phase VII.

A capacity term such as $I_{X_P}/(I_{X_P} + X_P)$ is an empirical approach to account for growth limitations beyond a certain size of the population, I_{X_P}, which may occur e.g. when biofilm thickness increases and diffusive mass transfer of reactants from the bulk aqueous phase penetrates only the upper biofilm layers (Barry et al. 2002). In this case, the specific growth rate is reduced, as only a fraction of the total biomass is exposed to substrates and usage of a capacity term avoids the need to explicitly simulate the diffusion across the biofilm (e.g. Kindred and Celia 1989; Zysset et al. 1994). Other studies consider capacity terms to account for inhibition by metabolic ecotoxins or spatial limitations in dense microbial populations (Wood and Dawson 1992) or simply to prevent unrealistic strong growth in situations of virtually unlimited substrate supply (Schäfer et al. 1998; Rolle et al. 2010). The maximum capacity can be estimated experimentally by measurement of bacteria concentrations in the biofilm at steady state and under conditions of high substrate loading (Zysset et al. 1994). Such measurements, however, have not been performed for the system studied here. I_{X_P} hence represents a fitting parameter and is required to prevent unrealistic excessive growth especially close to the tank inlet, where high concentrations of substrate are maintained throughout the experiment. The impact of the capacity parameter on the simulation results is evaluated in a sensitivity study ("Parameterization" section).

The isotope fractionation process, which commences with the inoculation of *A. aromaticum* EbN1 in experimental Phase VIII, was implemented in OGS following the concept of Van Breukelen and Prommer (2008), using individual components for the light and heavy fractions of the substrate in the reaction network. Therefore, the concentrations of both the unlabelled and labeled ethylbenzene fractions $C_8^1H_{10}$ and $C_8^2H_{10}$, which were injected as a 3:1 mixture, could be tracked individually and the spatial distribution of the isotopic ratios could be computed subsequently from the simulated concentrations of the two fractions. For isotope fractionation of ethylbenzene induced by anaerobic degradation via nitrate reduction by *A. aromaticum* EbN1 (X_A), the growth equation consists of contributions from both isotopologues (Van Breukelen and Prommer 2008).

$$\frac{dX_A}{dt} = \mu_{\max}^{A,C_8H_{10}} X_A \frac{NO_3^-}{M_{NO_3^-}^{A,C_8H_{10}} + NO_3^-} \frac{C_8{}^1H_{10}}{M_{C_8H_{10}}^{A} + C_8H_{10}} \frac{I_{X_A}}{I_{X_A} + X_A} + \mu_{\max}^{A,C_8H_{10}} X_A \frac{NO_3^-}{M_{NO_3^-}^{A,C_8H_{10}} + NO_3^-} \frac{C_8{}^2H_{10}}{M_{C_8H_{10}}^{A} + C_8H_{10}} \left(1 + \frac{\varepsilon}{1000}\right) \frac{I_{X_A}}{I_{X_A} + X_A} - \xi_A X_A \quad (8)$$

where NO_3^-, $C_8^1H_{10}$ and $C_8^2H_{10}$ are the concentrations of nitrate, labelled and unlabelled ethylbenzene isotopologues (mol m^{-3}), $M_{NO_3^-}^{A,C_8H_{10}}$ and $M_{C_8H_{10}}^{A}$ are the corresponding Monod concentrations (mol m^{-3}) for ethylbenzene degradation by *A. aromaticum* EbN1 via nitrate reduction, ε is the kinetic isotopic enrichment factor (–), I_{X_A} and ξ_A are the maximum capacity and decay rate coefficient for *A. aromaticum* EbN1, respectively. Note that inhibition of *A. aromaticum* EbN1 growth by oxygen is not included here. According to Eq. (8), $C_8^1H_{10}$ and $C_8^2H_{10}$ are simulated as two different reactive components.

The consumption of substrates S_i (electron donors and acceptors) is coupled to the growth equations [Eq. (7) or (8)] via

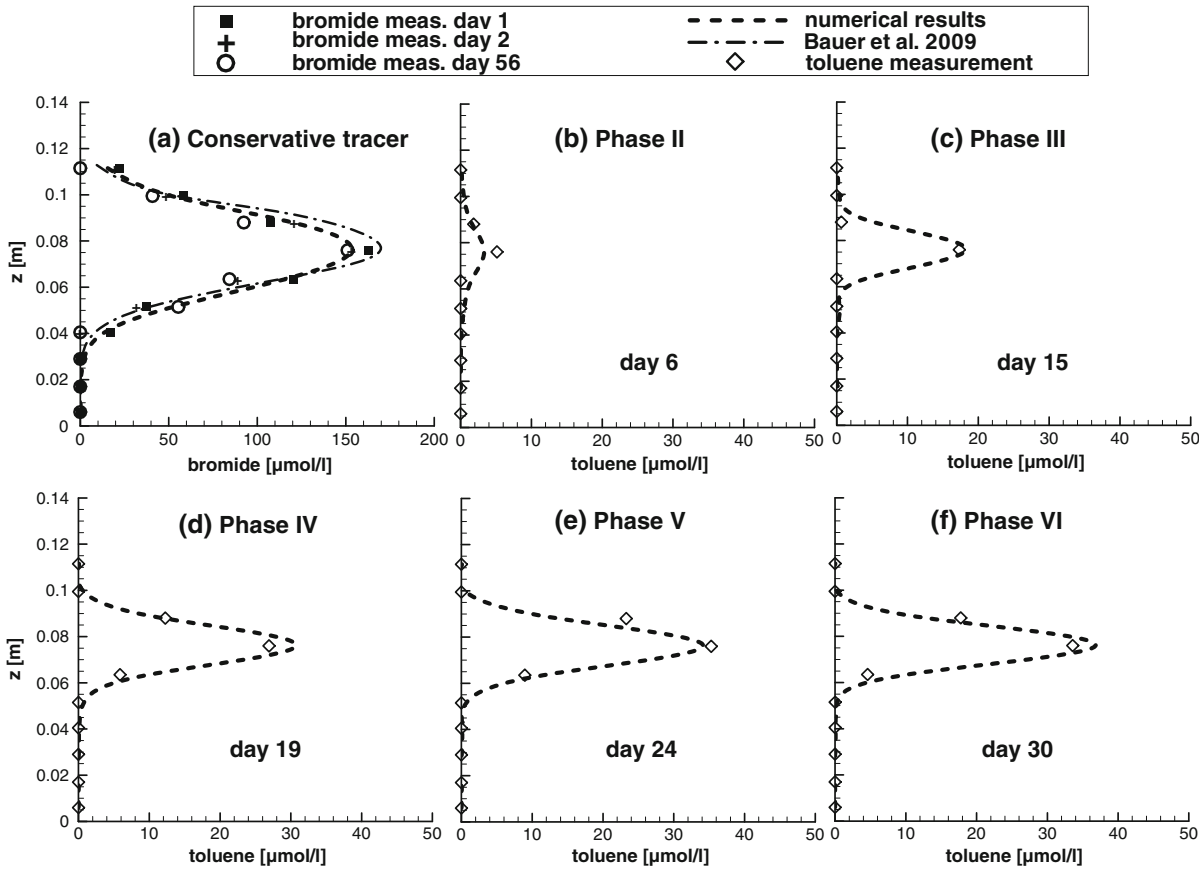

Fig. 3 Numerical results of the toluene distribution at the outlet ports for the first six phases of the experiment. For Phase I only bromide is reported, as no biodegradation was observed until the last day of the phase

$$\frac{dS_i}{dt} = \frac{-St_i}{Y_k^j}\left[\frac{dX_j}{dt}\right]_{growth} \tag{9}$$

where Y_k^j ($\mathrm{mol}_C\ \mathrm{mol}_{donor}^{-1}$) is the yield coefficient (related to the carbon assimilation efficiency) of the microorganism j (i.e. *P. putida* F1 or *A. aromaticum* EbN1) for the electron donor k (i.e. either toluene or ethylbenzene) and St_i (–) is the stoichiometric coefficient for substrate S_i of the electron donor/acceptor specific reaction equation. Note that in Eq. (9) for $C_8^1H_{10}$ and $C_8^2H_{10}$ and nitrate reduction, only the isotopologue specific contribution to growth of Eq. (8) is evaluated, respectively. The full sets of rate equations for all experimental phases are given in the Appendix.

Neither sorption, i.e. retardation, nor volatilization are accounted for in the numerical model. Also changes in porosity and hydraulic conductivity that could be induced by bioclogging were not considered, as under the specific experimental conditions the bacterial strains did not produce large amounts of extra-cellular polymeric substances as observed in other studies (e.g. Vandevivere and Baveye 1992; Thullner et al. 2002, 2004). In fact, as shown in Fig. 3a the distribution of the conservative tracer, which was constantly injected during the experiment, did not show any significant variations from day 1 to the end of Phase VIII that could be ascribed to temporal changes in the hydraulic properties of the porous medium. Also, the strongest clogging would take place close to the inlet ports where the nutrient concentrations are higher. As measurements are taken at the end of the tank (78 cm long), the overall effect on hydraulic conductivity would appear "diluted", as also reported in Thullner et al. (2002).

The high number of transported components and the inclusion of kinetically limited microbiological reactions results in an increased computational

demand; therefore, message passing interface (MPI) parallelization of the OGS flow, transport and reaction objects was implemented. MPI parallelization allows the decomposition of the finite element mesh into sub-domains, which can be distributed to individual processors of a high performance parallel computer (Wang et al. 2009). For kinetic reactions, the systems of coupled differential equations describing reactions at individual mesh nodes are independent from each other, and hence can be distributed to the multiple processors of the parallel computer to be solved simultaneously.

Parameterization

The flow and transport parameters introduced in the numerical model (Table 1) were considered as known parameters, as they were derived from the calibration of previous non-reactive tank experiments (Ballarini et al. 2012, 2013) performed in a porous medium with glass beads of same diameter (0.2–0.3 mm). In these experiments it was shown that a transfer of hydraulic parameters like porosity (n) or hydraulic conductivity (k) from one experiment to another is possible, if—as is the case here—experimental conditions are similar and the porous media are of the same grain size. Further details on the non reactive experiments, and a detailed sensitivity study on the impact of hydraulic parameters variation on the general transport behaviour, can be found in Ballarini et al. (2012, 2013). A sensitivity analysis on the impact of variations in hydraulic and transport parameters on the simulated electron donor and acceptor concentrations at the tank outlet ports and oxygen sensitive strips (i.e. the measurement data) was performed also in this study during the development of the numerical model. The

Table 1 Summary of transport and biokinetics parameters

Flow and transport parameters	Symbol	Unit	Value	
Porosity	n	–	0.42	
Hydraulic conductivity	k	m s^{-1}	1.70×10^{-3}	
Transverse dispersivity	α_T	m	1.48×10^{-5}/**5.0×10^{-5}**	
Longitudinal dispersivity	α_L	m	3.49×10^{-4}	
Aqueous diffusion coeff C_7H_8	D_{aq}	m^2 s^{-1}	8.49×10^{-10}	
Aqueous diffusion coeff $C_8^1H_{10}$	D_{aq}	m^2 s^{-1}	1.0082×10^{-9}	
Aqueous diffusion coeff $C_8^2H_{10}$	D_{aq}	m^2 s^{-1}	0.9613×10^{-9}	
Aqueous diffusion coeff O_2	D_{aq}	m^2 s^{-1}	2.10×10^{-9}	
Aqueous diffusion coeff NO_3^-	D_{aq}	m^2 s^{-1}	1.9×10^{-9}	
Biokinetic parameters	**Symbol**	**Unit**	***P. putida* F1**	***A. aromaticum* EbN1**
Maximum growth $rate_{Tol}$ constant	$\mu_{max}^{C_7H_8}$	s^{-1}	1.51×10^{-4}/**3.0×10^{-5}**	–
Maximum growth $rate_{Ethyl}$ constant	$\mu_{max}^{C_8H_{10}}$	s^{-1}	1.52×10^{-4}/**3.0×10^{-5}**	1.34×10^{-5}
Decay $rate_{Tol}$ constant	ξ	s^{-1}	-1.16×10^{-6}	–
Decay $rate_{Ethyl}$ constant	ξ	s^{-1}	-1.16×10^{-6}	-1.16×10^{-6}
Monod conc. for electron $donor_{Tol}$	$M_{C_7H_8}$	µmol l^{-1}	14	–
Monod conc. for electron $donor_{Ethyl}$	$M_{C_8H_{10}}$	µmol l^{-1}	10	11.4
Monod conc. for electron $acceptor_{Tol}$	$M_{O_2}^{C_7H_8}$	µmol l^{-1}	10	–
Monod conc. for electron $acceptor_{Ethyl}$	$M_{O_2}^{C_8H_{10}}$; $M_{NO_3^-}^{C_8H_{10}}$	µmol l^{-1}	3	70
Yield coeff. for electron $donor_{Tol}$	$Y_{C_7H_8}$	–	1.0 (0.143)[a]	–
Yield coeff. for electron $donor_{Ethyl}$	$Y_{C_8H_{10}}$	–	1.0 (0.125)[a]	1.0 (0.125)[a]
Capacity of X_i	I_{X_P}; I_{X_A}	µmol l^{-1}	1,000	1,000
Isotopic enrichment factor	ε	–	0	−545.7

Bold values represent the calibrated values

[a] Values in brackets denote carbon assimilation efficiency

results of this analysis, however, are rather straightforward and therefore it is only briefly summarized: increases in transverse dispersion (either by α_T or diffusion coefficient) result in increased mixing, stronger toluene/ethylbenzene degradation and hence in lower concentrations of the electron donors and acceptors, while variations in k or n only slightly affect the shape and position of electron donor/acceptor plumes in the concentration profiles.

Different batch experiments with *P. putida* F1 and *A. aromaticum* EbN1 were performed under oxic and anoxic conditions to derive the Monod half-saturation constants for toluene and ethylbenzene and the maximum growth rate of the two strains (Bauer et al. 2009a). On the other hand, the Monod coefficients for the electron acceptors (oxygen and nitrate) were assumed as fitting parameters (Bauer et al. 2008). Yield coefficients of about 1.4 mol microbial carbon produced per mol of substrate were observed on average for toluene degradation by *P. putida* F1 in oxic batch experiments, which corresponds to a carbon assimilation efficiency of 0.2. This value can be considerably lower for conditions of limited oxygen availability, as they occur during the tank experiments along the plume fringes. Carbon assimilation efficiency of anaerobic growth can be expected to be lower than for aerobic conditions, as this parameter is positively correlated with the free energy release of the catabolic pathway (Roden and Jin 2011). In contrast to oxygen, supplies of nitrate as electron acceptor for anaerobic degradation were not limiting degradation all over the plume during the experimental Phase VIII. Therefore, the yield coefficients for aerobic growth was assumed lower than that observed in the aerobic batch experiments and equal to 1.0 for both aerobic and anaerobic biodegradation (i.e. 1 mol of electron donor is required to produce 1 mol of microbial carbon, corresponding to carbon assimilation efficiencies of 0.143 in case of toluene and 0.125 in case of ethylbenzene). Isotope fractionation factors were also determined in batch experiments containing a similar mix of isotopologues and the respective bacterial strains (Bauer et al. 2009b). Growth kinetics parameters of the aerobic and anaerobic strains (*P. putida* F1 and *A. aromaticum* EbN1) considering toluene and ethylbenzene degradation are summarized in Table 1.

As mentioned above, the maximum capacities I_{X_j} are empirical and therefore unknown parameters. Their impact on the simulation results was evaluated in a sensitivity study, varying I_{X_j} within the range 100–100,000 in the aerobic (Phases I–VII) and competitive degradation phases (Phase VIII). The results, in terms of electron donor and acceptor concentration profiles (strips and outlet ports), are not sensitive on the maximum capacities for the first seven phases. For Phase VIII, however, small differences of few mm can be observed in the oxygen depleted plume width for different values of I_{X_j} (data not shown). Nevertheless, a capacity term within this range is required to reproduce the spatial pattern and the overall extent of anaerobic biodegradation indicated by the measured isotope ratios. In fact, without a maximum capacity, biomass would grow to unrealistic high values directly at the injection ports resulting in a complete degradation of ethylbenzene by *A. aromaticum* EbN1 due to the stoichiometric excess of nitrate. Hence, maximum capacities were set to a value of 1,000 for both microbial strains. These concentration levels are reached soon after the inoculation of the respective strains close to the injection port 7 (i.e. at day 5 in case of *P. putida* F1 and at day 50 in case of *A. aromaticum* EbN1).

Results and discussion

The numerical model focused on eight of the eleven phases that constitute the experiment, for a total amount of 56 simulated days. As nitrate concentrations were strongly increased in the injected groundwater after Phase VIII, ethylbenzene was almost completely degraded, and accordingly, no isotope fractionation could be measured. Therefore, no added insight or information can be gained from simulating the last experimental phases. Due to the stepwise increase of the injected carbon source concentration, the contaminant plume did not, in every case, reach steady state conditions within the individual phase. Therefore, the developed numerical model also tried to reproduce the transient behaviour of the plume by adjusting the kinetic parameters of the double Monod kinetic reaction (maximum growth rate and initial biomass concentration) used for the simulation of biodegradation, in order to avoid that steady-state is reached too fast compared to the experimental data. Each phase was simulated successively to the previous

one, using as initial conditions the computed distributions of the electron acceptors, the hydrocarbons and the biomass at the end of the previous experimental phase.

Evaluation of the aerobic degradation: Phases I–VI

Prior to the numerical evaluation of the experiment, a mass balance calculation of the experimental data of electron donor and acceptor was performed, assuming that only the aerobic toluene degradation reaction was taking place (Eq. 1). According to the stoichiometry of this reaction and the given oxygen and toluene inlet concentrations of 270 (all 10 inlet ports) and 50 μmol l^{-1} (plume inlet port 7), respectively, the mass flux of oxygen out of the tank measured for the six aerobic phases was found to be too low compared to the amount of toluene consumed. As the accuracy of the oxygen measurements during the experiment was verified by calibration measurements, this imbalance suggests that processes other than aerobic degradation of toluene (Eq. 1) might have resulted in a consumption of oxygen. Aerobic oxidation of ammonia, which is contained in the experimental groundwater medium with a concentration of 4.67 mmol l^{-1}, has been reported for *P. putida* strains (e.g. Daum et al. 1998; Bothe et al. 2000), but it is unlikely that this reaction caused the significant depletion suggested by the mass imbalance. An alternative explanation might be that the oxygen concentration in the injected plume and groundwater media was not maintained at 270 μmol l^{-1} during the course of the 74 days experiment. The oxygen concentrations of the injected water, however, have not been constantly monitored. Model simulations employing 270 μmol l^{-1} as injected oxygen concentration showed an almost complete degradation of toluene and a too narrow width of the oxygen depletion zone with some oxygen left in its center, which was not observed in the measured data. As a closed mass balance is an essential prerequisite for the application of the numerical model, the injected oxygen concentration in the model was assumed 180 μmol l^{-1}, which allowed a sufficiently accurate match of the experimental mass balance, and significantly improved the fits of the toluene plume and the oxygen depletion zone.

In the experiment no measurements were performed, which would allow for an integration of biomass attachment/detachment kinetics (e.g. Clement et al. 1997; Scheibe et al. 2007) in the numerical model (e.g. concentrations of suspended cells, bacterial breakthrough curves). Therefore, despite the inoculation process of the tank with *P. putida* F1 by injection through ports 6 and 8, in the numerical model the initial *P. putida* F1 distribution was conceptually simplified by defining an initially homogeneous distribution all over the tank. This was done in order to (notionally) permit growth of the bacteria everywhere in the tank and assuming that the biomass would quickly develop towards realistic spatial patterns following the distribution of the available substrates.

As mentioned above, the hydraulic parameters introduced in the numerical model were derived from previous conservative tracer tank experiments performed in a similar porous material (Ballarini et al. 2012, 2013). A breakthrough curve of the conservative tracer (bromide) was not measured during the experiment; therefore it was not possible to verify the correctness of the values assumed for n and α_L. Both parameters, however, only influence the plume shape during the transient phase by affecting the transport velocity and the plume length, therefore they were not included in the calibration. The vertical position of the anaerobic plume measured at the three oxygen sensitive strips (Fig. 4a–n) is sensitive on the hydraulic conductivity of the porous medium and was found to be appropriately reproduced with a k of 1.7×10^{-3} m s^{-1} taken from Ballarini et al. (2012). In contrast, the transverse dispersivity α_T reported in Ballarini et al. (2012) had to be increased to a value of 5.0×10^{-5} m, thus resulting in a very good fit of the bromide profile (Fig. 3a), improving the toluene distribution at the outlet ports (Fig. 3b–f), and providing an acceptable match of the anoxic plume width (Fig. 4a–n; note that no oxygen measurements for Phase VI were available). A possible explanation for the consistent underestimation of the width of the measured anaerobic plume core might be ascribed to the formation of gas bubbles (which were actually observed during the experiment) produced by microbial activity, which can distort the optical measurements. It must also be noted that within the same phase, the measured toluene concentrations varied considerably without a defined trend, while the simulated concentrations continuously approach steady state in each phase after few days. As neither the pumping rate, nor the contaminant concentration

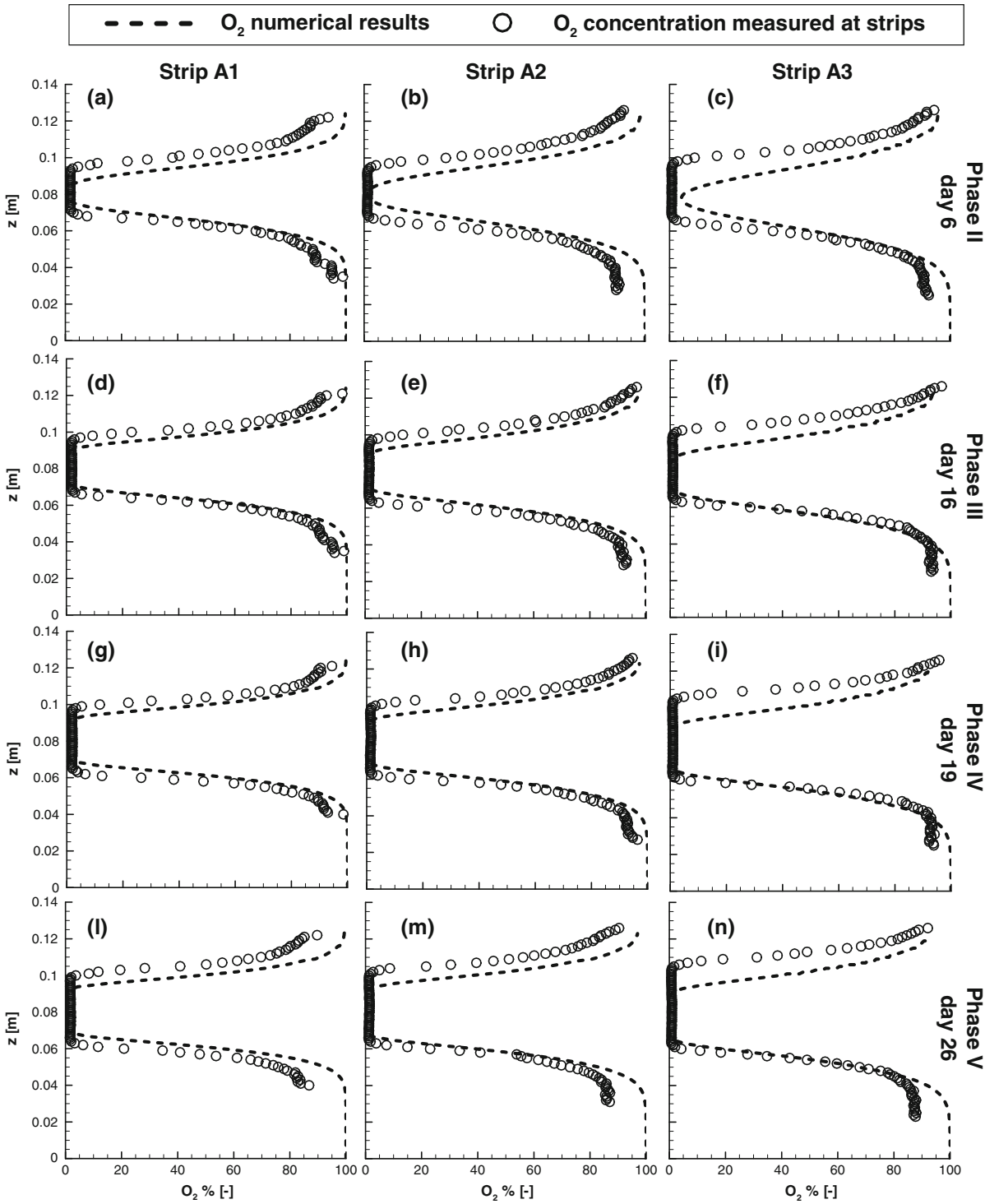

Fig. 4 Numerical results (Phase II–V) of the anoxic plume distribution compared to the oxygen measurements at the three strips. No oxygen measurements are available for Phase VI

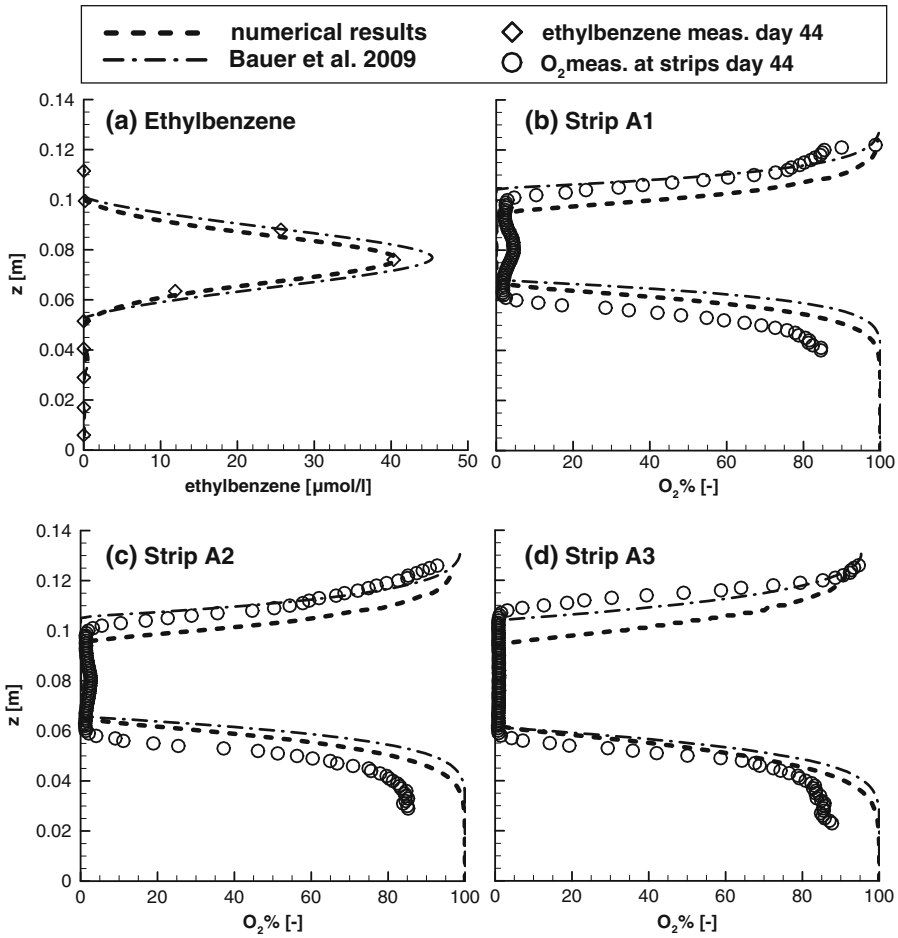

Fig. 5 Comparison of observed and simulated ethylbenzene (**a**) and oxygen (**b–d**) concentrations along the three sensitive strips during Phase VII

have been constantly monitored, it is possible that the boundary conditions might have changed during the same phase.

First, modeling results of the transient strain growth indicated that its growth rate was lower than the average growth rate constant of 1.51×10^{-4} s^{-1} determined in previously performed batch experiments. As already discussed by Bauer et al. (2009b), this is not unexpected because parameters resulting from idealized and closed batch systems with complete mixing between electron donor and acceptor often are not valid when investigating natural processes in porous media. Except for Phase I, where no biodegradation was observed until the last day of the phase (day 4), all the other phases of the experiment could be satisfactorily reproduced with the same set of parameters using a maximum growth rate constant of 3.0×10^{-5} s^{-1} (Figs. 3, 4). The measurements reported in the figures refer to specific points in time when both oxygen and the electron donor were measured (or close days if both measurements were not taken at the same day).

Change of electron donor: Phase VII

In Fig. 5, exemplary results of the numerical evaluation of Phase VII (days 37–46) are shown and compared to the numerical model of Bauer et al. (2009a). Regarding the ethylbenzene concentrations at the tank outlet, it must be noted that the measurements at the tank outlet are not at steady-state. Despite that, the numerical results showed a good agreement to the last measurements of ethylbenzene (day 44, Fig. 5a), when concentrations are more stable.

Compared to the previous phase, the measured anaerobic plume is 4 mm wider, and although ethylbenzene has an 18 % higher aqueous diffusion coefficient than toluene, the numerical results indicate a

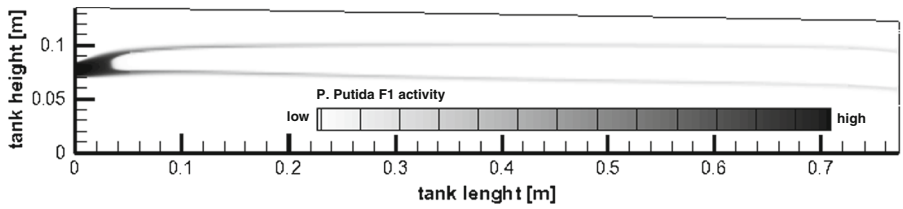

Fig. 6 *P. putida* F1 activity after 36 days of toluene and 9 days of ethylbenzene injection into oxic groundwater medium

narrower anaerobic area (Fig. 5b–d) compared to the measured data. The *P. putida* F1 biomass distribution at the end of Phase VII, resulting from the calibrated numerical model, is reported in Fig. 6. The model shows preferential growth of the bacteria close to the inlet, where oxygen and ethylbenzene are both injected and available at high concentrations, and along the fringe of the oxygen depleted plume, where the electron acceptor is provided by transverse mixing from the ambient groundwater. The simulated distribution is somewhat idealized, as at the beginning of the experiment, the biomass concentrated more at the inlet and inoculation ports (ports 6 and 8), as well as along the plume fringes. Along with growing, however, the biomass spreads all over the tank within several days as observed in similar experiments (Bauer et al. 2008, 2009b). Zones of highest biomass still are close to the inlet and along the fringes of the plume, but considerable amounts of cells can be found also within the oxygen depleted core of the plume.

Evaluation of the competitive aerobic and anaerobic biodegradation: Phase VIII

The distributions of ethylbenzene, O_2 and *P. putida* F1 obtained from numerical simulation of the previous phase at day 46 were used as initial conditions for the simulation of Phase VIII.

Numerical results were compared to the measurements of ethylbenzene, isotope fractionation and NO_3^- at the outlet ports and O_2 measured at the oxygen sensitive strips as indication of aerobic degradation activity. In the first model simulations, similar to the modeling of the aerobic degradation phases, a uniform distribution of the *A. aromaticum* EbN1 biomass was considered as a simplified initial condition. We assumed that the biomass would quickly develop towards realistic spatial patterns, but the strong initial shift in the isotopic ratio observed at the outlet ports 6 and 8 already one day after the inoculation could not be reproduced successfully. The immediate and strong fractionation in ports 6 and 8 was interpreted in Bauer et al. (2009a) as an indication of anaerobic biodegradation mainly at the plume fringes due to transverse mixing. Nevertheless, the model results highlighted that the nitrate concentration in the plume core is actually sufficient to completely degrade the ethylbenzene left-over from the aerobic degradation. A plausible explanation for the strong isotope shift detected already one day after the inoculation may be found in the initial spatial distribution of the bacteria in the experiment. The inoculation of the anaerobic strain through the two ports directly above and below the contaminant injection port is probable to have produced a biomass distribution focussed at the plume fringes. In order to verify this theory, such an initial distribution of the microbes was reproduced in the numerical model in order to provide a more realistic initial biomass distribution, i.e. the initial biomass was increased along the injection zone of the tank.

Figures 7, 8 and 9 show exemplary results from the numerical evaluation of Phase VIII, while Fig. 10 shows the *A. aromaticum* EbN1 distribution at the end of Phase VIII considering the effect of the inoculation process. Compared to Phase VII, the measured anaerobic plume is wider, although the ethylbenzene in excess should be consumed by the anaerobic process. Therefore, the numerical results do not fit the width of the oxygen depleted plume (Fig. 7a–c). The simulated isotopic patterns (Fig. 8) were very sensitive on the assumed initial distribution of the *A. aromaticum* EbN1 biomass after the inoculation. The simulated and measured isotopologue ratios showed a good reproduction of the measurements for day 47 and 51 (Fig. 8a, b), indicating that the inoculation process, and hence the initial biomass distribution, at least in part explains the strong initial fractionation at the plume fringes. The increase in the biodegradation dynamics in the core of the plume observed in the final

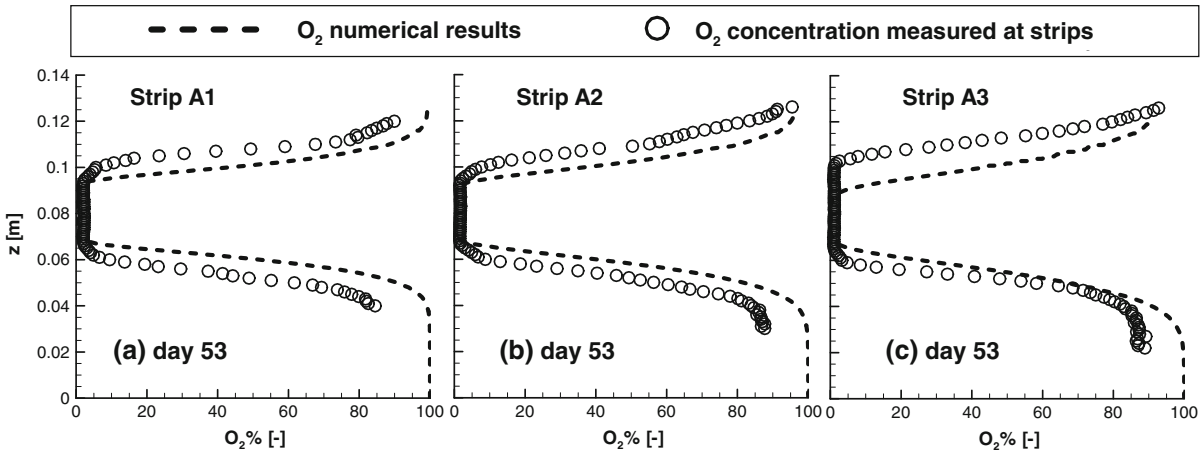

Fig. 7 Comparison of observed and simulated oxygen distribution (**a**–**c**) during Phase VIII of the experiment

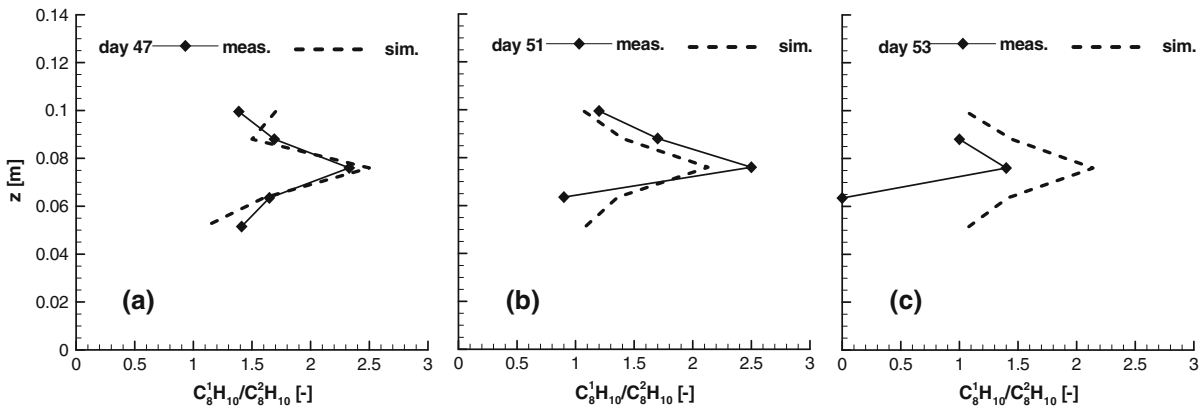

Fig. 8 Comparison between the observed and simulated ratios of labelled and unlabelled ethylbenzene during Phase VIII of the experiment

isotope measurements on day 53 was not fully reproduced by the numerical model (Fig. 8c), while ethylbenzene and nitrate concentrations (Fig. 9a–f) both fit the measurements well.

The observed ethylbenzene concentration decreased already during the first day after the inoculation but did not reach a steady level during the observation period (Fig. 9a–c). From day 47 until day 52, ethylbenzene concentrations and isotopologue ratios remained on a rather constant level. On day 53, measured concentrations decreased considerably, which was accompanied by a decrease in the isotopologue ratio at the plume fringes and in the core of the plume (Figs. 8c; 9c). Ethylbenzene degradation increased further until the end of Phase VIII (data not shown). The numerical model was able to properly reproduce the ethylbenzene distribution and its general transience. In Fig. 9 only comparisons for day 47, 51 and 53 (coinciding with the isotope measurements) are reported.

Similarly, comparison of measured and simulated nitrate concentrations (Fig. 9d–f) showed a good agreement for days 48 (no nitrate measurements were taken on days 47), 51 and 52 (figure not shown). Also, until day 51 Eq. (3), representing the process of complete conversion of nitrate to nitrogen, was implemented in the numerical model to reproduce the anaerobic degradation of ethylbenzene, but the strong depletion in nitrate observed after day 52 could only be reproduced switching to Eq. (4). The same problem was described in Bauer et al. (2009a), where it was hypothesized that the actual stoichiometry of the reaction could be an intermediate between both

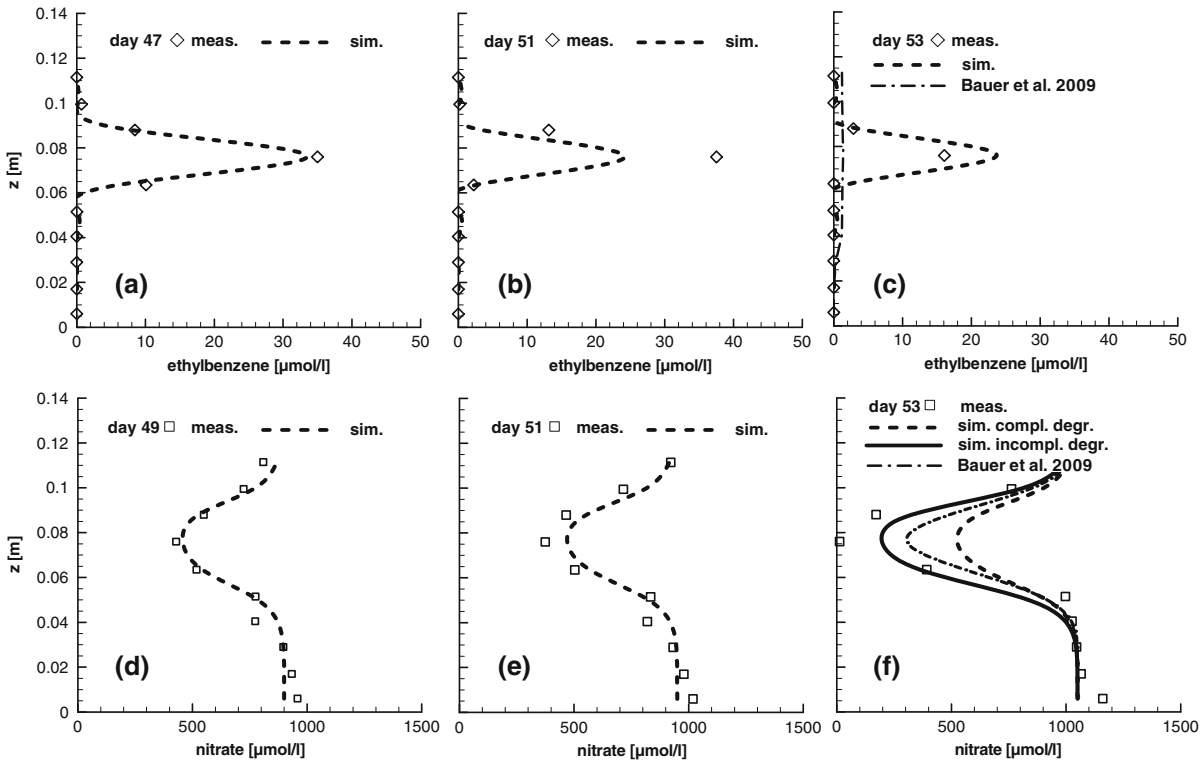

Fig. 9 Comparison of observed and simulated ethylbenzene concentrations (**a**–**c**), and nitrate concentrations (**d**–**f**) during Phase VIII of the experiment

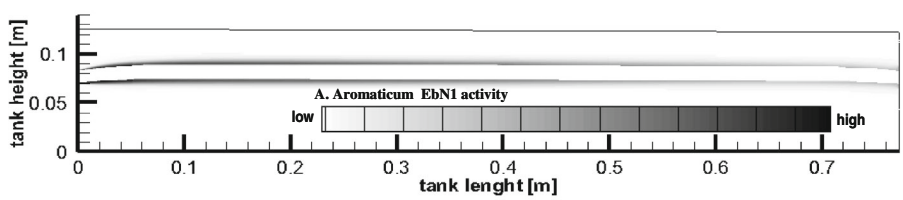

Fig. 10 *A. aromaticum* EbN1 activity considering an initial distribution limited to the fringes caused by the inoculation process

equations. In fact, the reaction of Eq. (4) stoichiometrically requires 150 % more nitrate than Eq. (3) to degrade one mol of the electron donor. A comparison between nitrate consumed using both reactions and the results of the numerical model of Bauer et al. (2009a) is reported in Fig. 9f.

Generally, in case of biodegradation only one reaction is dominant and changes from one to another degradation pathway may happen if the surrounding conditions change (Wöhlbrand et al. 2007). In the batch experiments performed before the tank experiment, *A. aromaticum* EbN1 produced nitrite as long as nitrate concentrations were sufficiently high, while a complete conversion of nitrate to nitrogen via intermediate products nitrite and nitrous oxide was observed under conditions of lower nitrate concentrations. In the flow through tank, both situations and hence both reaction stoichiometries (and transitions between them) may occur with spatially and temporally changing extent. During the first few days of Phase VIII, the inoculated biomass is probably situated mainly close to the injection ports in the left hand side of the tank. Due to the low concentration of nitrate injected together with the ethylbenzene in port 7, the complete conversion of nitrate via Eq. 3 might be the dominant reaction. Transverse mixing of high nitrate concentrations from the groundwater medium injected through the other ports into the plume requires the

transport over some distance in the porous medium. Therefore, zones where mainly nitrite is produced from ethylbenzene biodegradation may favourably be located in the right hand side of the tank. As bacterial transport and the population of the complete tank by *A. aromaticum* EbN1 requires some time, dominance of reaction Eq. 4 might develop after several days, as observed in the measurement data. Still, with both reaction stoichiometries the model predictions do not reproduce the strong depletion of nitrate in the core of the plume, i.e. at outlet port 7, although the measurements at the plume fringes are matched very well assuming Eq. 4. Obviously, the dynamics of biomass growth in the core of the plume are a key factor for the temporal changes observed between days 51 and 53 in all measurements. This dynamic is not well captured by the numerical model with the assumptions made for initial biomass distributions and biomass decay under conditions of low substrate concentrations. The simulated distribution of *A. aromaticum* EbN1 biomass (Fig. 10) hence probably is only a good approximation for the first few days of Phase VIII.

The actual spatial biomass concentration was measured in three sediment samples collected over vertical profiles located at the oxygen sensitive strip positions at the end of the experiment (after phase XI). Although simplified, the model still reproduces the main biomass distribution patterns postulated in Bauer et al. (2009a, b; two peeks at the plume fringes), with the exception of the population in the plume core close to the tank outlet observed in Bauer et al. (2009b), which does not fit the degradation activity indicated by the isotope measurements. Note, however, that after experimental Phase VIII, nitrate was injected to the plume medium through port 7 in high concentrations allowing for a complete degradation of the ethylbenzene, obviously causing strong growth of biomass in the core of the plume. Also, chemotactic movement, as observed in a very similar experimental tank setup by Strobel et al. (2011) may have contributed to the population of the plume core. It must be noted that the Monod model Eq. (8) with a simple first order rate as a sink term for bacterial decay does not allow capturing processes such as inactivation or dormancy of the biomass under conditions of substrate depletion or unfavourable growth conditions (e.g. Jin and Bethke 2007; Stolpovsky et al. 2011). Another limitation is the simplified representation of the inoculation process by assuming a likely distribution of *A. aromaticum* EbN1 as initial condition for Phase VIII, instead of explicitly simulating bacterial spreading and attachment/detachment. As explained above, however, the experiment lacked the necessary measurements of bacterial cell breakthrough curves to allow a parameterization of this process. Consequently, the simulated distributions (Fig. 6 and 10) should be interpreted as a measure of biomass activity involved in contaminant break down rather than the absolute biomass present.

Summary and conclusions

In this paper, high resolution reactive transport modeling was applied for a model based evaluation of a complex and transient laboratory experiment focusing on the evolution of a transient toluene plume (Phase I–VI), which was later replaced by a 3:1 mixture of unlabelled and fully deuterated ethylbenzene isotopologues (Phase VII). Competitive aerobic and anaerobic biodegradation, with oxygen and nitrate as electron acceptors, was then performed by a mixed culture of two microbial strains, the aerobic strain *P. putida* F1 and the denitrifying strain *A. aromaticum* EbN1 (Phase VIII). The calibrated numerical model was able to reproduce the measured transient evolution of the electron donor and acceptor concentrations reasonably well over the eight simulated phases of the experiment, while fluctuations of concentrations observed within some of the individual phases were not fully captured. The model also included the fractionation of ethylbenzene isotopologues induced by *A. aromaticum* EbN1. A very strong fractionation observed at the fringes at the beginning of experimental Phase VIII indicates that processes other than transverse mixing driven biodegradation at the fringes need to be considered. The spatio-temporal evolution of the isotope pattern hence could only be reproduced taking into account the inoculation process of the anaerobic strain. Previous modeling work of Bauer et al. (2009a) did not identify this problem, as the hybrid analytical - numerical model concept used did not include the fractionation process.

In this way, this work demonstrates that the complex transient lab-scale experiment, mimicking the interaction of processes to be expected at BTEX contaminated sites (i.e. coupled groundwater flow, transient multicomponent transport and mixing limited aerobic/anaerobic degradation by competing microbial populations) can be parameterized and quantitatively simulated at a

satisfying level of accuracy by a calibrated numerical reactive transport model. Still, open questions remain e.g. with respect to the correct pathways and stoichiometries of the denitrification process, as already discussed in Bauer et al. (2009a). As nitrate is an important electron acceptor for BTEX contaminants, more insight on the spatio-temporal evolution and extent of denitrification reactions in groundwater contaminant plumes is necessary. Also, the modeling analysis shows that the conceptual models typically used to describe bacterial dynamics coupled to transport processes and groundwater contaminant biodegradation at contaminated sites have room for improvement with respect to bacterial behaviour under stress conditions or active spreading of motile biomass driven by geochemical gradients. Though model concepts exist to quantitatively describe these processes, their integration and parameterization in field scale biodegradation models is still a task to accomplish.

Acknowledgments This work is a cooperation within the research group "Reaction in porous media" (FOR 525/2) funded by the Deutsche Forschungsgemeinschaft.

Appendix

The biogeochemical system of the tank experiments consists of the different components of the artificial groundwater medium ($NaHCO_3$, Na_2SO_4, NaCl, KCl, $MgCl_2$-hexahydrate, NH_4Cl, KH_2PO_4, $CaCl_2$-dihydrate, trace elements, vitamins, $NaNO_3$, O_2; see Bauer et al. (2008) for details), further species represented in the reaction equations describing microbial metabolism from aerobic toluene and aerobic/anaerobic ethylbenzene degradation (cf. reaction Eqs 1–4) as well as reaszurine and KBr, which were used as redox indicator and conservative tracer, respectively. For the numerical simulations, however, only a fraction of these components or species had to be simulated explicitly, as most nutrients were available in excess quantities and concentrations of some of the reaction products were not measured. Table 2 gives an overview of the different mobile and immobile components considered in the numerical model of the tank experiments.

The ordinary differential equations (ODE) used for describing microbial metabolism coupled to consumption of substrates and production of reaction products in the numerical model can be derived from Eqs. (1)–(9) as follows:

Table 2 Components and species considered in the numerical simulations

Toluene	C_7H_8	Mobile
Ethylbenzene	$C_8^1H_{10}$	Mobile
Deuterated ethylbenzene	$C_8^2H_{10}$	Mobile
Oxygen	O_2	Mobile
Nitrate	NO_3^-	Mobile
Nitrite	NO_2^-	Mobile
Nitrogen	N_2	Mobile
Bicarbonate	HCO_3^-	Mobile
Bromide	Br^-	Mobile
Pseudomonas putida F1	$CH_{1.8}O_{0.5}N_{0.2}$	Immobile
Aromatoleum aromaticum EbN1	$CH_{1.8}O_{0.5}N_{0.2}$	Immobile

During experimental Phases I–VI, aerobic degradation of toluene (Eq. 1) by *P. putida* F1 is modelled by four rate equations, i.e.,

$$\frac{dX_P}{dt} = r_1 = \mu_{\max}^{P,C_7H_8} X_P \frac{O_2}{M_{O_2}^{P,C_7H_8} + O_2} \frac{C_7H_8}{M_{C_7H_8}^{P} + C_7H_8} \frac{I_{X_P}}{I_{X_P} + X_P} - \xi X_P \tag{10}$$

$$\frac{dC_7H_8}{dt} = r_2 = -\frac{St_{C_7H_8}}{Y_{C_7H_8}^{P}} \mu_{\max}^{P,C_7H_8} X_P \frac{O_2}{M_{O_2}^{P,C_7H_8} + O_2} \frac{C_7H_8}{M_{C_7H_8}^{P} + C_7H_8} \frac{I_{X_P}}{I_{X_P} + X_P} \tag{11}$$

$$\frac{dO_2}{dt} = r_3 = -\frac{St_{O_2}}{Y_{C_7H_8}^{P}} \mu_{\max}^{P,C_7H_8} X_P \frac{O_2}{M_{O_2}^{P,C_7H_8} + O_2} \frac{C_7H_8}{M_{C_7H_8}^{P} + C_7H_8} \frac{I_{X_P}}{I_{X_P} + X_P} \tag{12}$$

$$\frac{dHCO_3^-}{dt} = r_4 = \frac{St_{HCO_3^-}}{Y_{C_7H_8}^{P}} \mu_{\max}^{P,C_7H_8} X_P \frac{O_2}{M_{O_2}^{P,C_7H_8} + O_2} \frac{C_7H_8}{M_{C_7H_8}^{P} + C_7H_8} \frac{I_{X_P}}{I_{X_P} + X_P} \tag{13}$$

In experimental Phase VII, toluene is replaced by a mixture of deuterated and non-deuterated ethylbenzene. Aerobic degradation of ethylbenzene (Eq. 2) by *P. putida* F1 then is modelled by a set of five rate equations:

$$\frac{dX_P}{dt} = r_5 = \mu_{\max}^{P,C_8H_{10}} X_P \frac{O_2}{M_{O_2}^{P,C_8H_{10}} + O_2} \frac{C_8{}^1H_{10} + C_8{}^2H_{10}}{M_{C_8H_{10}}^{P} + C_8{}^1H_{10} + C_8{}^2H_{10}} \frac{I_{X_P}}{I_{X_P} + X_P} - \xi X_P \quad (14)$$

$$\frac{dC_8{}^1H_{10}}{dt} = r_6 = -\frac{St_{C_7H_8}}{Y_{C_8H_{10}}^{P}} \mu_{\max}^{P,C_8H_{10}} X_P \frac{O_2}{M_{O_2}^{P,C_8H_{10}} + O_2} \frac{C_8{}^1H_{10}}{M_{C_8H_{10}}^{P} + C_8{}^1H_{10} + C_8{}^2H_{10}} \frac{I_{X_P}}{I_{X_P} + X_P} \quad (15)$$

$$\frac{dC_8{}^2H_{10}}{dt} = r_7 = -\frac{St_{C_7H_8}}{Y_{C_8H_{10}}^{P}} \mu_{\max}^{P,C_8H_{10}} X_P \frac{O_2}{M_{O_2}^{P,C_8H_{10}} + O_2} \frac{C_8{}^2H_{10}}{M_{C_8H_{10}}^{P} + C_8{}^1H_{10} + C_8{}^2H_{10}} \frac{I_{X_P}}{I_{X_P} + X_P} \quad (16)$$

$$\frac{dO_2}{dt} = r_8 = -\frac{St_{O_2}}{Y_{C_8H_{10}}^{P}} \mu_{\max}^{P,C_8H_{10}} X_P \frac{O_2}{M_{O_2}^{P,C_8H_{10}} + O_2} \frac{C_8{}^1H_{10} + C_8{}^2H_{10}}{M_{C_8H_{10}}^{P} + C_8{}^1H_{10} + C_8{}^2H_{10}} \frac{I_{X_P}}{I_{X_P} + X_P} \quad (17)$$

$$\frac{dHCO_3^-}{dt} = r_9 = \frac{St_{HCO_3^-}}{Y_{C_8H_{10}}^{P}} \mu_{\max}^{P,C_8H_{10}} X_P \frac{O_2}{M_{O_2}^{P,C_8H_{10}} + O_2} \frac{C_8{}^1H_{10} + C_8{}^2H_{10}}{M_{C_8H_{10}}^{P} + C_8{}^1H_{10} + C_8{}^2H_{10}} \frac{I_{X_P}}{I_{X_P} + X_P} \quad (18)$$

After the inoculation of the denitrifying strain *A. aromaticum* EbN1 in Phase VIII, aerobic and anaerobic degradation of deuterated and non-deuterated ethylbenzene proceed simultaneously, which for the case of complete denitrification of nitrate to nitrogen (Eq. 3) leads to the following set of rate equations:

$$\frac{dX_P}{dt} = r_5 \quad (19)$$

$$\frac{dX_A}{dt} = r_{10} = \mu_{\max}^{A,C_8H_{10}} X_A \frac{NO_3^-}{M_{NO_3^-}^{A,C_8H_{10}} + NO_3^-} \left[\frac{C_8{}^1H_{10} + C_8{}^2H_{10}(1+\varepsilon/1000)}{M_{C_8H_{10}}^{A} + C_8{}^1H_{10} + C_8{}^2H_{10}}\right] \frac{I_{X_A}}{I_{X_A} + X_A} - \xi X_A \quad (20)$$

$$r_{11} = -\frac{St_{C_8H_{10}}}{Y_{C_8H_{10}}^{A}} \mu_{\max}^{A,C_8H_{10}} X_A \frac{NO_3^-}{M_{NO_3^-}^{A,C_8H_{10}} + NO_3^-} \frac{C_8{}^1H_{10}}{M_{C_8H_{10}}^{A} + C_8{}^1H_{10} + C_8{}^2H_{10}} \frac{I_{X_A}}{I_{X_A} + X_A} \quad (21)$$

$$r_{12} = -\frac{St_{C_8H_{10}}}{Y_{C_8H_{10}}^{A}} \mu_{\max}^{A,C_8H_{10}} X_A \frac{NO_3^-}{M_{NO_3^-}^{A,C_8H_{10}} + NO_3^-} \frac{C_8{}^2H_{10}(1+\varepsilon/1000)}{M_{C_8H_{10}}^{A} + C_8{}^1H_{10} + C_8{}^2H_{10}} \frac{I_{X_A}}{I_{X_A} + X_A} \quad (22)$$

$$\frac{dC_8{}^1H_{10}}{dt} = r_6 + r_{11} \quad (23)$$

$$\frac{dC_8{}^2H_{10}}{dt} = r_7 + r_{12} \quad (24)$$

$$\frac{dO_2}{dt} = r_8 \quad (25)$$

$$\frac{dNO_3^-}{dt} = r_{13} = -\frac{St_{NO_3^-}}{Y_{C_8H_{10}}^{A}} \mu_{\max}^{A,C_8H_{10}} X_A \frac{NO_3^-}{M_{NO_3^-}^{A,C_8H_{10}} + NO_3^-} \left[\frac{C_8{}^1H_{10} + C_8{}^2H_{10}(1+\varepsilon/1000)}{M_{C_8H_{10}}^{A} + C_8{}^1H_{10} + C_8{}^2H_{10}}\right] \frac{I_{X_A}}{I_{X_A} + X_A} \quad (26)$$

$$\frac{dN_2}{dt} = r_{14} = \frac{St_{N_2}}{Y_{C_8H_{10}}^{A}} \mu_{\max}^{A,C_8H_{10}} X_A \frac{NO_3^-}{M_{NO_3^-}^{A,C_8H_{10}} + NO_3^-} \left[\frac{C_8{}^1H_{10} + C_8{}^2H_{10}(1+\varepsilon/1000)}{M_{C_8H_{10}}^{A} + C_8{}^1H_{10} + C_8{}^2H_{10}}\right] \frac{I_{X_A}}{I_{X_A} + X_A} \quad (27)$$

$$r_{15} = \frac{St_{HCO_3^-}}{Y_{C_8H_{10}}^{A}} \mu_{\max}^{A,C_8H_{10}} X_A \frac{NO_3^-}{M_{NO_3^-}^{A,C_8H_{10}} + NO_3^-} \left[\frac{C_8{}^1H_{10} + C_8{}^2H_{10}(1+\varepsilon/1000)}{M_{C_8H_{10}}^{A} + C_8{}^1H_{10} + C_8{}^2H_{10}}\right] \frac{I_{X_A}}{I_{X_A} + X_A} \quad (28)$$

$$\frac{dHCO_3^-}{dt} = r_9 + r_{15} \quad (29)$$

For the case incomplete denitrification of nitrate to nitrite (Eq. 4) the following set of rate equations applies:

$$\frac{dX_P}{dt} = r_5 \quad (30)$$

$$\frac{dX_A}{dt} = r_{10} \quad (31)$$

$$\frac{d\mathrm{C_8{}^1H_{10}}}{dt} = r_6 + r_{11} \tag{32}$$

$$\frac{d\mathrm{C_8{}^2H_{10}}}{dt} = r_7 + r_{12} \tag{33}$$

$$\frac{d\mathrm{O_2}}{dt} = r_8 \tag{34}$$

$$\frac{dNO_3^-}{dt} = r_{16} = -\frac{St_{\mathrm{NO_3^-}}}{Y^A_{\mathrm{C_8H_{10}}}}\mu^{A,\mathrm{C_8H_{10}}}_{\max} X_A \frac{\mathrm{NO_3^-}}{M^{A,\mathrm{C_8H_{10}}}_{\mathrm{NO_3^-}} + \mathrm{NO_3^-}} \left[\frac{\mathrm{C_8{}^1H_{10}} + \mathrm{C_8{}^2H_{10}}(1+\varepsilon/1000)}{M^A_{\mathrm{C_8H_{10}}} + \mathrm{C_8{}^1H_{10}} + \mathrm{C_8{}^2H_{10}}}\right] \frac{I_{X_A}}{I_{X_A} + X_A} \tag{35}$$

$$\frac{d\mathrm{NO_2^-}}{dt} = r_{17} = \frac{St_{\mathrm{NO_2^-}}}{Y^A_{\mathrm{C_8H_{10}}}}\mu^{A,\mathrm{C_8H_{10}}}_{\max} X_A \frac{\mathrm{NO_3^-}}{M^{A,\mathrm{C_8H_{10}}}_{\mathrm{NO_3^-}} + \mathrm{NO_3^-}} \left[\frac{\mathrm{C_8{}^1H_{10}} + \mathrm{C_8{}^2H_{10}}(1+\varepsilon/1000)}{M^A_{\mathrm{C_8H_{10}}} + \mathrm{C_8{}^1H_{10}} + \mathrm{C_8{}^2H_{10}}}\right] \frac{I_{X_A}}{I_{X_A} + X_A} \tag{36}$$

$$\frac{d\mathrm{HCO_3^-}}{dt} = r_9 + r_{15}. \tag{37}$$

References

Ballarini E, Bauer S, Eberhardt C, Beyer C (2012) Evaluation of transverse dispersion effects in tank experiments by numerical modeling: parameter estimation, sensitivity analysis and revision of experimental design. J Contam Hydrol 134–135:22–36

Ballarini E, Bauer S, Eberhardt C, Beyer C (2013) Evaluation of the role of heterogeneities on transverse mixing in bench-scale tank experiments by numerical modeling. Ground Water. doi:10.1111/gwat.12066

Barry DA, Prommer H, Miller CT, Engesgaard P, Brun A, Zheng C (2002) Modelling the fate of oxidisable organic contaminants in groundwater. Adv Water Res 25(8–12): 945–983

Bauer S, Beyer C, Kolditz O (2006) Assessing measurement uncertainty of first-order degradation rates in heterogeneous aquifers. Water Resour Res. doi:10.1029/2004WR003878

Bauer RD, Maloszewski P, Zhang Y, Meckenstock RU, Griebler C (2008) Mixing-controlled biodegradation in a toluene plume—results from two-dimensional laboratory experiments. J Contam Hydrol 96:150–168

Bauer RD, Rolle M, Bauer S, Eberhardt C, Grathwohl P, Kolditz O, Meckenstock RU, Griebler C (2009a) Enhanced biodegradation by hydraulic heterogeneities in petroleum hydrocarbon plumes. J Contam Hydrol 105:56–68

Bauer RD, Rolle M, Bauer S, Kürzinger P, Grathwohl P, Meckenstock RU, Griebler C (2009b) Two-dimensional flow-through microcosms—versatile test systems to study biodegradation processes in porous aquifers. J Hydrol 369:284–295

Beyer C, Chen C, Gronewold J, Kolditz O, Bauer S (2007) Determination of first-order degradation rate constants from monitoring networks. Ground Water 45(6):774–785

Beyer C, Konrad W, Rügner H, Bauer S, Liedl R, Grathwohl P (2009) Model based prediction of long-term leaching of contaminants from secondary materials in road constructions and noise protection dams. Waste Manag 29:839–850

Blum P, Hunkeler D, Weede M, Beyer C, Grathwohl P, Morasch B (2009) Quantification of biodegradation for o-xylene and naphthalene using first order decay models, Michaelis–Menten kinetics and stable carbon isotopes. J Contam Hydrol 105:118–130

Bockelmann A, Zamfirescu D, Ptak T, Grathwohl P, Teutsch G (2003) Quantification of mass fluxes and natural attenuation rates at an industrial site with a limited monitoring network: a case study. J Contam Hydrol 60(1–2):97–121

Bothe H, Jost G, Schloter M, Ward BB, Witzel K (2000) Molecular analysis of ammonia oxidation and denitrification in natural environments. FEMS Microbiol Rev 24:673–690

Centler F, Shao H, De Biase C, Park CH, Regnier P, Kolditz O, Thullner M (2010) GeoSysBRNS—a flexible multidimensional reactive transport model for simulating biogeochemical subsurface processes. Comput Geosci 36(3):397–405

Chapelle FH, Bradley PM, Lovley DR, Vroblesky DA (1996) Measuring rates of biodegradation in a contaminated aquifer using field and laboratory methods. Ground Water 34(4):691–698

Clement TP, Peyton BM, Skeen RS, Jennings DA, Petersen JN (1997) Microbial growth and transport in porous media under denitrification conditions: experiments and simulations. J Contam Hydrol 24(3–4):269–285

Daum M, Zimmer W, Papen H, Kloos K, Nawrath K, Bothe H (1998) Physiological and molecular biological characterization of ammonia oxidation of the heterotrophic nitrifier pseudomonas putida. Curr Microbiol 37(4):281–288

Declercq I, Cappuyns V, Duclos Y (2012) Monitored natural attenuation (MNA) of contaminated soils: state of the art in Europe—a critical evaluation. Sci Total Environ 426:393–405

Gillham RW, Starr RG, Miller DJ (1990) A device for in situ determination of geochemical transport parameters, 2: biochemical reactions. Ground Water 28:858–862

Huang WE, Oswald SE, Lerner DN, Smith CC, Zheng C (2003) Dissolved oxygen imaging in a porous medium to investigate biodegradation in a plume with limited electron acceptor supply. Environ Sci Tech 37(9):1905–1911

Hunkeler D, Anderson N, Aravena R, Bernasconi SM, Buttler BJ (2001) Hydrogen and carbon isotope fractionation during aerobic biodegradation of benzene. Environ Sci Technol 35:3462–3467

Hunkeler D, Aravena R, Berry-Spark K, Cox E (2005) Assessment of degradation pathways in an aquifer with mixed chlorinated hydrocarbon contamination using stable isotope analysis. Environ Sci Technol 39:5975–5981

Jin Q, Bethke CM (2007) The thermodynamics and kinetics of microbial metabolism. Am J Sci 307:643–677

Kindred JS, Celia MA (1989) Contaminant transport and biodegradation: 2. Conceptual model and test simulations. Water Resour Res 25(6):1149–1159

Kleerebezem R, van Loosdrecht MCM (2010) A generalized method for thermodynamic state analysis of environmental systems. Crit Rev Environ Sci Technol 40:1–54

Klenk ID, Grathwohl P (2002) Transverse vertical dispersion in groundwater and the capillary fringe. J Contam Hydrol 58(1–2):111–128

Kolditz O, Bauer S (2004) A process-oriented approach to computing multi-field problems in porous media. J Hydroinf 6(3):225–244

Kolditz O, Bauer S, Bilke L, Böttcher N, Delfs JO, Fischer T, Görke UJ, Kalbacher T, Kosakowski G, McDermott CI (2012a) OpenGeoSys: an open-source initiative for numerical simulation of thermo-hydro-mechanical/chemical (THM/C) processes in porous media. Environ Earth Sci 67(2):589–599. doi:10.1007/s12665-012-1546-x

Kolditz O, Görke UJ, Shao H, Wang W (2012b) Thermo-hydro-mechanical-chemical processes in porous media: benchmarks and examples (lecture notes in computational science and engineering). Springer, Berlin

Li D, Bauer S, Benisch K, Graupner B, Beyer C (2013) OpenGeoSys-ChemApp: a coupled simulator for reactive transport in multiphase systems: code development and application at a representative CO_2 storage formation in Northern Germany. Acta Geotech. doi:10.1007/s11440-013-0234-7 (in print)

Mancini SA, Ulrich CA, Lacrampe-Couloume G, Sleep B, Edwards EA, Sherwood Lollar B (2003) Carbon and hydrogen isotopic fractionation during anaerobic biodegradation of benzene. Appl Environ Microbiol 69:191–198

Meckenstock RU, Morasch B, Warthmann R, Schink B, Annweiler E, Michaelis W, Richnow HH (1999) $^{13}C/^{12}C$ isotope fractionation of aromatic hydrocarbons during microbial degradation. Environ Microbiol 1:409–414

Meckenstock RU, Morasch B, Griebler C, Richnow HH (2004) Stable isotope fractionation analysis as a tool to monitor biodegradation in contaminated acquifers. J Contam Hydrol 75:215–255

Morasch B, Richnow HH, Schink B, Meckenstock RU (2001) Stable hydrogen and carbon isotope fractionation during microbial toluene degradation: mechanistic and environmental aspects. Appl Environ Microbiol 67:4842–4849

Morasch B, Richnow HH, Schink B, Vieth A, Meckenstock RU (2002) Carbon and hydrogen stable isotope fractionation during aerobic bacterial degradation of aromatic hydrocarbons. Appl Environ Microbiol 68:5191–5194

Nambi IM, Werth CJ, Sanford RA, Valocchi AJ (2003) Pore-scale analysis of anaerobic halo-respiring bacterial growth along the transverse mixing zone of an etched silicon pore network. Environ Sci Tech 37(24):5617–5624

Olsson A, Grathwohl P (2007) Transverse dispersion of non-reactive tracers in porous media: a new nonlinear relationship to predict dispersion coefficients. J Contam Hydrol 92:149–161

Peter A, Steinbach A, Liedl R, Ptak T, Michaelis W, Teutsch G (2004) Assessing microbial degradation of *o*-xylene at field-scale from the reduction in mass flow rate combined with compound-specific isotope analyses. J Contam Hydrol 71:127–154

Rabus R, Widdel F (1995) Anaerobic degradation of ethylbenzene and other aromatic hydrocarbons by new denitrifying bacteria. Arch Microbiol 163:96–103

Rein A, Bauer S, Dietrich P, Beyer C (2009) Influence of temporally variable groundwater flow conditions on point measurements and contaminant mass flux estimations. J Contam Hydrol 108:118–133

Roden EE, Jin Q (2011) Thermodynamics of microbial growth coupled to metabolism of glucose, ethanol, short-chain organic acids, and hydrogen. Appl Environ Microbiol 77:1907–1909

Rolle M, Chiogna G, Bauer R, Griebler C, Grathwohl P (2010) Isotopic fractionation by transverse dispersion: flow-through microcosms and reactive transport modeling study. Environ Sci Technol 44:6167–6173

Schäfer D, Schäfer W, Kinzelbach W (1998) Simulation of reactive processes related to biodegradation in aquifers: 1. Structure of the three-dimensional reactive transport model. J Contam Hydrol 31(1–2):167–186

Scheibe TD, Dong H, Xie Y (2007) Correlation between bacterial attachment rate coefficients and hydraulic conductivity and its effect on field-scale bacterial transport. Adv Water Resour 30(6–7):1571–1582

Schmidt TC, Zwank L, Elsner M, Berg M, Meckenstock RU, Haderlein SB (2004) Compound-specific stable isotope analysis of organic contaminants in natural environments—a critical review of state of the art, prospects and future challenges. Anal Bioanal Chem 378:283–300

Sherwood Lollar B, Slater GF, Ahad J, Sleep B, Spivack J, Mackenzie P, Brennan M (1999) Contrasting carbon isotope fractionation during biodegradation of trichloroethylene and toluene: implications for intrinsic bioremediation. Org Geochem 30:813–820

Stelzer N, Büning C, Pfeifer F, Dohrmann AB, Tebbe CC, Nijenhuis I, Kästner M, Richnow HH (2006) In situ microcosms to evaluate natural attenuation potentials in contaminated aquifers. Org Geochem 37:1394–1410

Stolpovsky K, Martinez-Lavanchy P, Heipieper HJ, Van Cappellen P, Thullner M (2011) Incorporating dormancy in dynamic microbial community models. Ecol Model 222(17):3092–3102

Strobel KL, McGowan S, Bauer RD, Griebler C, Liu J, Ford RM (2011) Chemotaxis increases vertical migration and apparent transverse dispersion of bacteria in a bench-scale microcosm. Biotechnol Bioeng 108:2070–2077

Thornton SF, Quigley S, Spence MJ, Banwart SA, Bottrell S, Lerner DN (2001) Processes controlling the distribution and natural attenuation of dissolved phenolic compounds in a deep sandstone aquifer. J Contam Hydrol 53:233–267

Thullner M, Mauclaire L, Schroth MH, Kinzelbach W, Zeyer J (2002) Interaction between water flow and spatial distribution of microbial growth in a two-dimensional flow field in saturated porous media. J Contam Hydrol 58:169–189

Thullner M, Schroth MH, Zeyer J, Kinzelbach W (2004) Modeling of a microbial growth experiment with bioclogging in a two-dimensional saturated porous media flow field. J Contam Hydrol 70:37–62

Tuxen N, Albrechtsen HJ, Bjerg PL (2006) Identification of a reactive degradation zone at a landfill leachate plume fringe using high resolution sampling and incubation techniques. J Contam Hydrol 85:179–194

Van Breukelen BM, Prommer H (2008) Beyond the Rayleigh equation: reactive transport modeling of isotope fractionation effects to improve quantification of biodegradation. Environ Sci Technol 42(7):2457–2463

Vandevivere P, Baveye P (1992) Effect of bacterial extracellular polymers on the saturated hydraulic conductivity of sand columns. Appl Environ Microbiol 58(5):1690–1698

Wang W, Kosakowski G, Kolditz O (2009) A parallel finite element scheme for thermo-hydro-mechanical (THM) coupled problems in porous media. Comput Geosci 35:1631–1641

Watson IA, Oswald SE, Banwart SA, Crouch RS, Thornton SF (2005) Modeling the dynamics of fermentation and respiratory processes in a groundwater plume of phenolic contaminants interpreted from laboratory- to field-scale. Environ Sci Technol 39:8829–8839

Wiedemeier TH, Rifai HS, Wilson TJ, Newell C (1999) Natural attenuation of fuels and chlorinated solvents in the subsurface. Wiley, Hoboken

Wöhlbrand L, Kallerhoff B, Lange D, Hufnage P, Thiermann J, Reinhardt R, Rabus R (2007) Functional proteomic view of metabolic regulation in Aromatoleum aromaticum strain EbN1. Proteomics 7:2222–2239

Wood BD, Dawson CN (1992) Effects of lagand maximum growth in contaminant transport and biodegradation modeling. Mathematical Modeling in Water Resources

Zysset A, Stauffer F, Dracos T (1994) Modeling of reactive groundwater transport governed by biodegradation. Water Resour Res 30(8):2423–2434